Thuane T. da Silva[1], Matheus P. Ribeiro[1],*
Lucas de M. Neuba[1], Ana P. da Silva[2], Sergio N. Monteiro[1],
Marcos P. C. de Medeiros[1], Lucio F. C. Nascimento[1]

[1]Department of Materials Science, Military Institute of Engineering — IME, Praça General Tibúrcio 80, Urca, Rio de Janeiro-RJ, Brazil
[2]Brazilian Navy Research Institute—IPqM, Materials Technology Group; Rua Ipiru, 02, Cacuia, Rio de Janeiro-RJ, Brazil

Scientific paper
ISSN 0351-9465, E-ISSN 2466-2585
https://doi.org/10.62638/ZasMat1478

Zastita Materijala 67 ()
(2026)

Chemical and thermal analysis of flax, aramid, and aluminum for HDPE composites in protective helmets

ABSTRACT

An increasing interest in the use of sustainable materials as reinforcements in polymer composites is observed, including for ballistic helmets used by the military forces. Typical examples are natural lignocellulosic fibers (NLFs), applied as reinforcement of lightweight, economical, and environmentally friendly composites compared to synthetic fibers such as glass, carbon, and aramid. Their physical and mechanical properties vary according to the origin and characteristics of the fibers, influencing their applications. Hybridization enhances the properties of composites, leading to the investigation of various reinforcement materials. The present study characterizes aluminum, as well as fabrics of flax, a NLF, and aramid, combined with high-density polyethylene (HDPE), as the composite matrix using fourier transform infrared spectroscopy (FTIR), x-ray diffraction (XRD), thermogravimetric analysis (TGA), and differential scanning calorimetry (DSC) for possible application as hybrid composites. In the FTIR analysis, the materials presented functional groups compatible with those described in the literature. Additionally, aramid and HDPE showed higher crystallinity values of approximately 69% and 83%, respectively. From TGA and DSC results, it was possible to determine the individual working temperature of the materials, which was about 200 °C, and consider it for the possible composites. These findings are compatible with the requirements for ballistic helmets associated with radiological protections.
Keywords: *Characterization; Fourier Transform Infrared Spectroscopy; X-Ray Diffractogram; Thermogravimetric Analysis; Differential Scanning Calorimetry.*

1. INTRODUCTION

The growing demand for materials with specific properties and lower environmental impact has driven research into the development of polymer composites reinforced with natural lignocellulosic fibers (NLFs). This class of materials offers a wide range of application possibilities, thanks to the sustainability and versatility of NLFs and polymer matrices [1–5].

NLFs, with their diverse physical and mechanical properties, have been widely explored as reinforcements in polymer composites [6,7]. Compared to synthetic fibers, NLFs, such as flax, display relevant advantages in terms of lower density, cost effectiveness, and zero environmental impact, making them an attractive option for various applications [8, 9].

Aramid, a synthetic fiber, stands out because of its low density combined with its high specific strength and modulus, making it an extremely strong material. With their high specific strength, stiffness, and low density, flax fiber offers new possibilities for innovative applications in composite materials, providing a sustainable alternative [6,10,11].

Likewise, hybridization has proven to be an effective way to enhance the properties of composites. Therefore, research on the use of different types of materials, specifically NLFs, as reinforcements has become common in recent years [12–16]. Hybrid composite materials are used in numerous situations related to wide temperature variations. It is crucial to analyze their thermal behavior, as significant temperature differences can impact the structural stability of these composites. The thermal properties of hybrid composites are determined by both the nature and characteristics of the polymer and the reinforcement materials [17–20]. The twaron, made of aramid fibers, exhibits excellent heat resistance

*Corresponding author: Matheus P. Ribeiro
E-mail: eng.matheuspribeiro@gmail.com
Paper received: 02. 06.2025.
Paper accepted: 12. 06.2025.

and dimensional stability, characteristics that make it ideal for a wide range of applications [21].

Ballistic impact armors are essential in the design and development of military gears. A ballistic helmet is one of the primary pieces of personal protective equipment for soldiers and police officers. Reports show that the use of ballistic helmets effectively reduces the casualty rate of soldiers on the battlefield by 19% [22–25]. Although the head and neck represent only 12% of a human body, head injuries account for half of combat fatalities. In a non-penetrating ballistic impact, a significant amount of kinetic energy is transferred to the brain parenchyma within the helmet due to the rapid deceleration of the bullet in a confined space, which can result in traumatic brain injuries [22,26–28].

Regarding the ballistic and shrapnel effects of bombs, military personnel specialized in chemical, biological, radiological, and nuclear (CBRN) defense, as well as civilians and public security forces responsible for the first response to CBRN threats, are also exposed to the danger of so-called "dirty bombs", which combine conventional explosives with radioactive materials. The personal protective equipment currently available for this type of mission is limited to providing ballistic protection, neglecting the necessary radiological protection when confronting "dirty bombs". Therefore, there is a critical need for the research and development of materials that combine lightness and protection against all threats, including radiation, to enable soldiers to carry out their missions safely and effectively.

In this context, the present work proposes the investigation of materials, including aluminum, flax, aramid, and high-density polyethylene (HDPE) for possible novel hybrid composites and technologies for the manufacturing of ballistic helmets that also provide radiological protection. The primary objective is to combine the ballistic properties of aramid, the sustainable, lightweight, and mechanically efficient attributes of flax fabrics, as well as the reasonable absorption of Cesium 137 radiation by aluminum plates, to further develop hybrid composites capable of meeting the demanding requirements of military personnel in high-risk operations.

2. EXPERIMENTAL

2.1. Materials

2.1.1. Flax Fabric

The flax fabric, as shown in Figure 1, was supplied from Casa Carlos Ltda, Brazil, in 1.5 x 25 m² rolls. For the production of composites, the plain weave fabric was cut into 12 x 15 cm² layers and dried in an oven at 60 °C for 24 h. The density adopted for the fibers was approximately 1.3 g/cm³ [2].

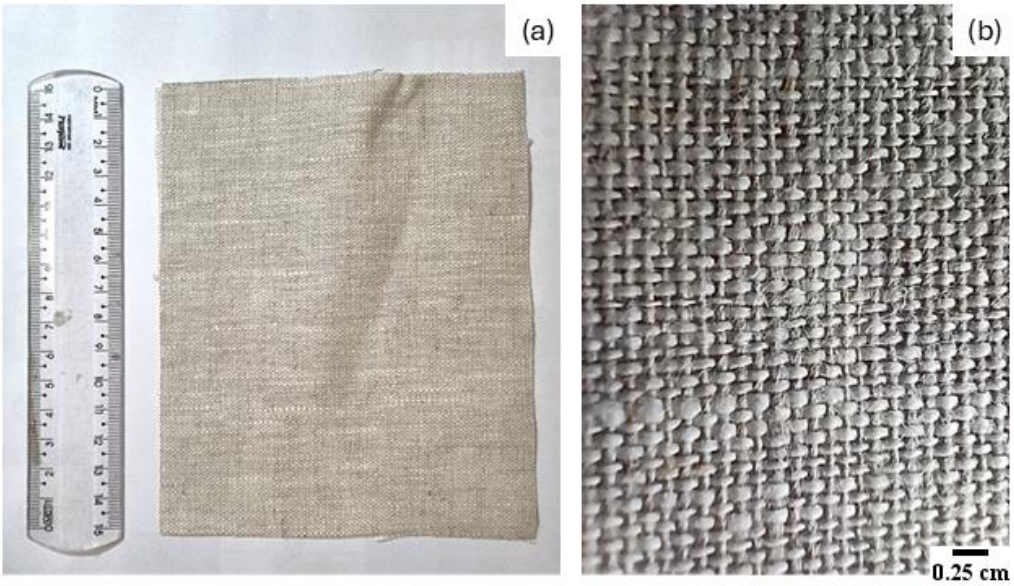

Figure 1. Flax fabric: (a) size 12 x 15 cm; (b) enlargement of the weave

2.1.2. Aramid Fabric

In this research, the aramid fabric adopted was Twaron CT 736 fabric, supplied by Teijin. It was used with a 2 x 2 basket weave, weight of 410 g/m², thickness of 2 mm and density of 1.41 g/cm³. For the production of composites, the fabrics were cut into 12 cm x cm pieces. Figure 2 shows the fabric cut in 12 x 15 cm² size.

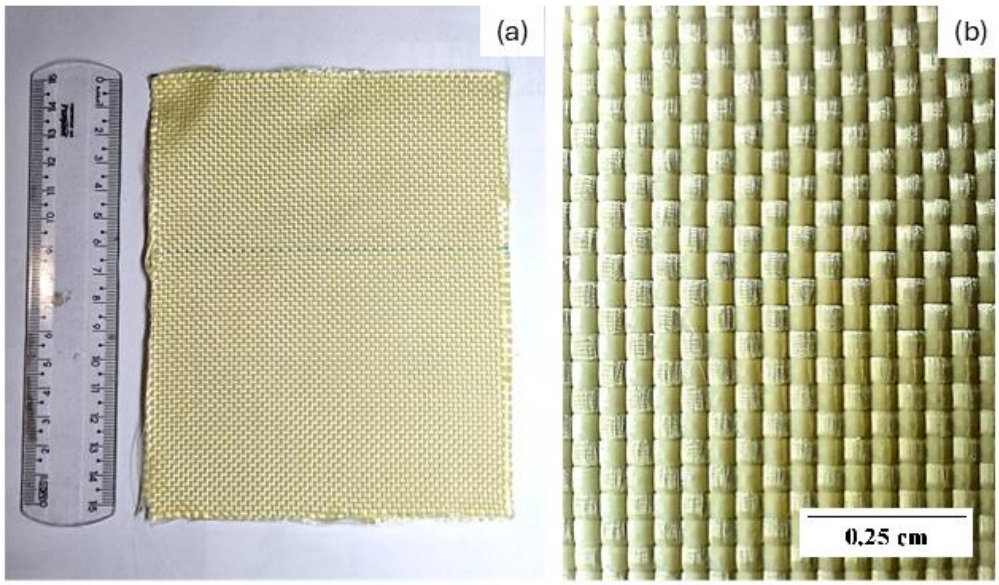

Figure 2. Aramid fabric: (a) size 12 x 15 cm; (b) enlargement of the weave

2.1.3. High-Density Polyethylene (HDPE)

The HDPE used in this work is HDPE HE150, which was supplied by Braskem SA, Brazil. In Figure 3 the material is presented as received for the production of the composite.

In Table 1 the listed properties of the HDPE supplied for the present work are presented.

Table 1. HDPE properties of the supplied material used in the present work

Properties	
Density	0.948 g/cm³
Shore-D Hardness	62
Flexural Modulus	1280 MPa
Tensile Strength	40 MPa
Melting Point	128

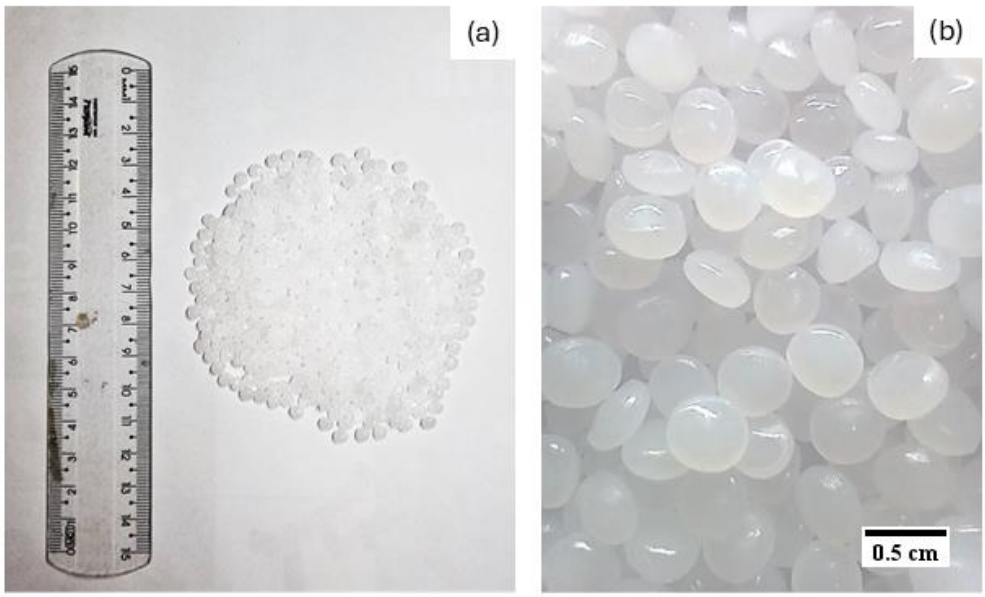

Figure 3. HDPE pellets (a) as received for the composite production; (b) enlargement

2.1.4. Aluminum Plates

The aluminum plates used in this study were purchased from Expansão Metal Ltda, Brazil. The plates were purchased in 12 x 15 cm², with a mesh of 3 x 4 mm² and a density of 2.7 g/cm³. Figure 4 shows the as-received plates.

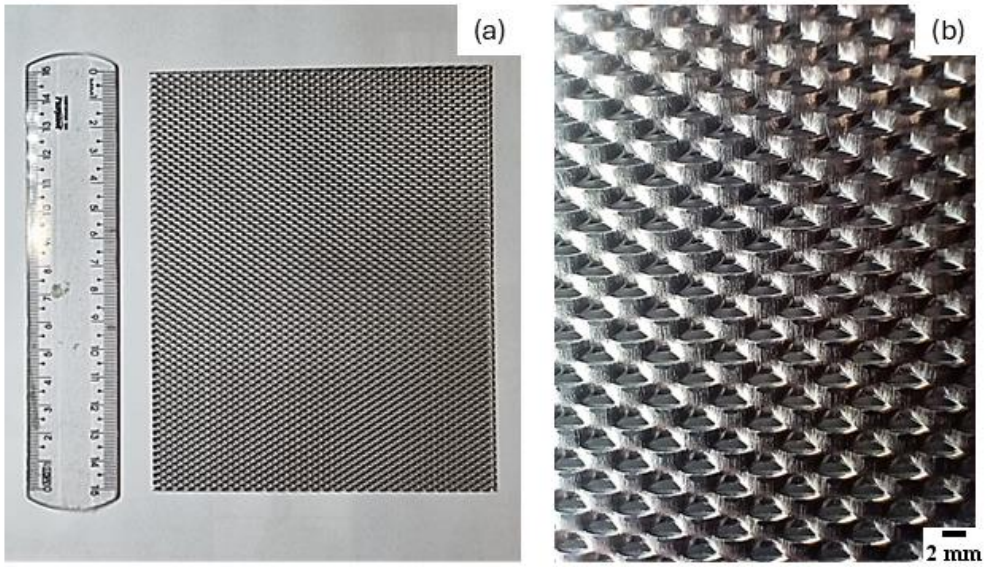

Figure 4. Aluminum: (a) size 12 x 15 cm; (b) mesh enlargement.

2.2. Methods

2.2.1. Determination of Grammage

According to ASTM D3776-20 [29], five 100 cm² test specimens were each cut using a metal plate. The mass of these samples was determined using a Mettler PM 460 analytical balance and the grammage, in g/cm², was calculated from the average mass of the samples by the area value of the samples.

2.2.2. Fourier Transform Infrared Spectroscopy (FTIR)

Fourier Transform Infrared Spectroscopy analysis was conducted using a Nicolet FT-IR spectrometer from Thermo Scientific in the Thin Films and Asphaltic Surfaces Laboratory (PEMM) at UFRJ. The FTIR test was performed in the wavenumber range of to 4000 cm^{-1}.

2.2.3. X-Ray Diffractogram (XRD)

XRD was used to determine the phases and crystalline structures within the materials. This technique relies on the scattering of X-rays as they interact with atoms, which may be arranged in a crystalline lattice. The intensities of the reflected beams and the interplanar spacings are measured according to Bragg's law [30,31]. Also, these values were employed to assess the crystallinity index of natural fibers.

It was carried out using a PANalyticalXPert Pro MRD System with CuKα radiation, in the Materials Science and Engineering Section of the Military Institute of Engineering (IME). The 2θ scan range was 5-80 for polymers and fabrics, and 5-120 for aluminum, with a scan speed of 2θ/5s for all samples.

As for the Crystallinity Index (CI), Segal et al. [32] developed an empirical method that allows us to estimate the degree of crystallinity in cellulosic materials by analyzing the relationship between the intensity peaks of the crystalline regions and the amorphous halo.

This method for measuring the degree of crystallinity has been widely employed in the analysis of lignocellulosic materials. Through fitting techniques, it is possible to measure the interference intensity in the crystalline plane (002) and the amorphous scattering at 2θ = 18◦ [32,33]. Thus, the crystallinity index can be calculated using Eq. 1:

$$C_I = \frac{A_{cr}}{A_{cr} + A_{am}} . 100 \quad (1)$$

CI is a parameter that indicates the amount of cellulose present in a crystalline state in lignocellulosic materials. This index plays an important role in the determination of the mechanical properties of these materials. From this value, it is possible to infer whether the material is more dense or less dense, since higher crystallinity corresponds to fewer void spaces [33].

2.2.4. Thermogravimetric Analysis (TGA)

Thermogravimetric analysis was performed on the aramid and flax fabrics, aluminum plates and HDPE pellets. A sample for each group was comminuted and placed in open platinum crucibles.

The test was carried out as specified in ASTM E1131-20. The equipment, belonging to the Naval Research Institute (IPqM), was a Shimadzu DTG-

60H model which operates in a nitrogen atmosphere. The samples were subjected to a heating rate of 10 ◦C/min, with a temperature range of 20 to 900 ◦C.

2.2.5. Differential Scanning Calorimetry (DSC)

DSC analysis was performed on aramid and flax fabrics, aluminum plates, HDPE pellets, and composites, using one sample of each material and composition. The test was carried out at the Navy Research Institute (IPqM), Brazil. The samples were comminuted and placed in a closed platinum crucible, except for aluminum, which was tested in an open crucible, in a Shimadzu DSC-60 device. The operation was carried out in a nitrogen atmosphere with a heating rate of 10 ◦C/min, within a temperature range of 20 to 600 ◦C.

3. RESULTS

3.1. Determination of Grammage

The results obtained from the grammage analysis of the fabric materials are presented in Table 2.

Table 2. Values analyzed from mass, thickness and weight of the materials studied

Sample	Mass (g)	Thickness (mm)	Grammage (g/m²)
Flax	2.53 ± 0.04	0.45 ± 0.02	252.92
Aramid	4.16 ± 0.46	0.55 ± 0.03	416.02

The data presented in Table 2 indicates a lighter flax fabric compared to the synthetic textile adopted, as a coarser aramid fabric is commonly adopted in ballistic helmets. Proportionally, a thicker aramid fabric will imply a material with a higher grammage, which indicates that, disregarding mechanical resistance for now, a single layer of aramid fabric could be equivalent to multiple layers of flax fabric. This was observed in previous work of hybrid composite materials [34,35].

3.2. X-ray Diffraction (XRD)

In Figure 5 the diffractograms obtained for the flax fabric (a), aramid fabric (b), HDPE (c) and aluminum plate (d) are presented by computational processing of data using software OriginLab.

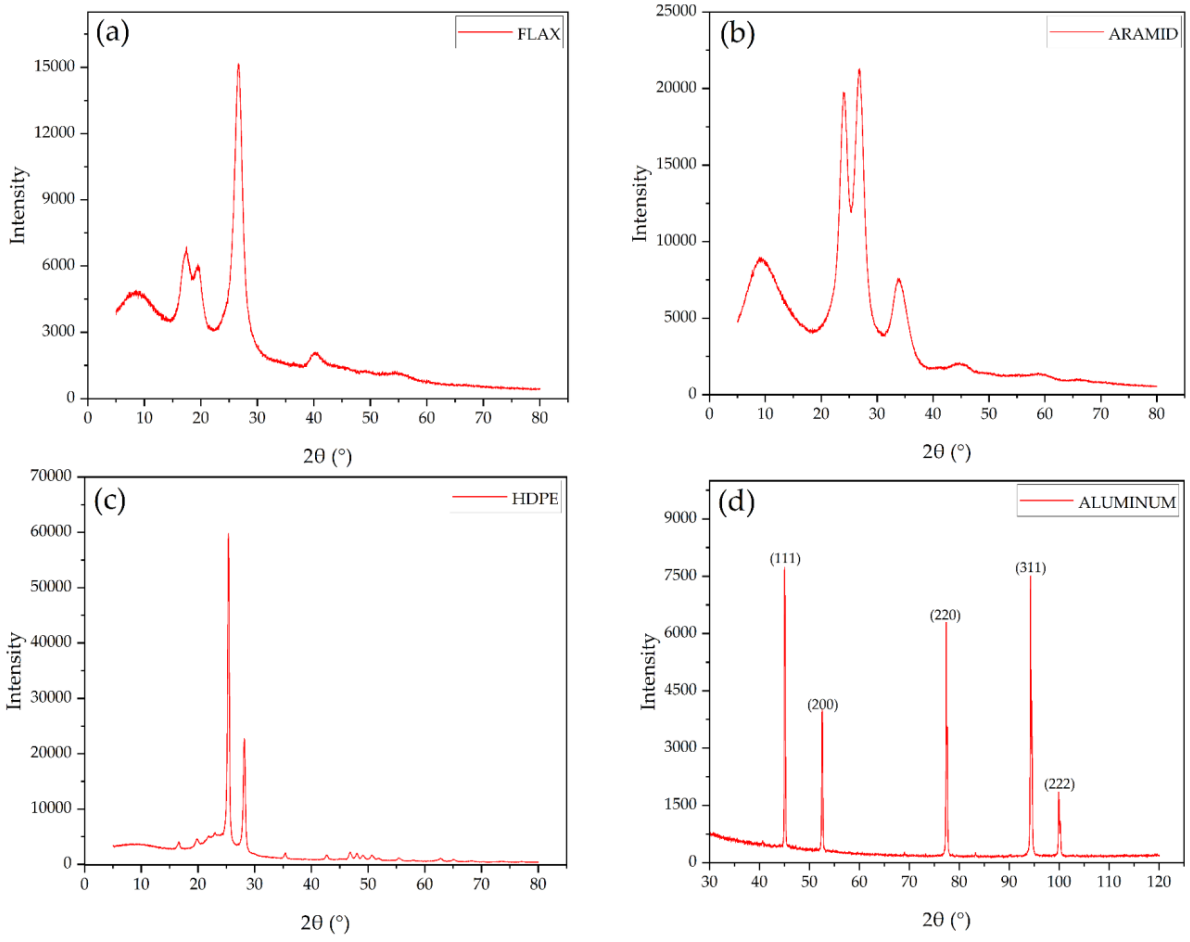

Figure 5. XRD diffractogram of: (a) flax fabric; (b) aramid fabric; (c) HDPE; (d) aluminum plate

The mechanical properties of NLFs are significantly influenced by the corresponding crystallinity index (Ic), which is one of the essential factors to consider [36]. To determine Ic of the flax fiber, Figure 5(a), the area under the curves related to the cellulosic crystalline material was calculated and applied to Equation 1 together with that related to a lower intensity associated with a lower crystallinity level of NLF. As a result, Ic of approximately 69% was obtained for the flax fabric, supporting the results found in the literature [37,38].

It is known that a number of factors influence the properties of NLFs, which explains the different crystallinities reported in the literature, ranging from 64% to 75%.

Figure 5(b) shows the diffractogram obtained for the aramid fabric. From the lower and higher peaks obtained from the diffractogram, it was possible to calculate the Ic of the aramid fabric. The calculation yielded a Ic value of about 69% for the Twaron fabric adopted, which is between what was reported before for different aramid fabrics, such as 55.3% for Kevlar 29 [36], and about 80% for Twaron750D [39].

Figure 5(c) shows the diffractogram obtained for the HDPE sample. The Ic obtained from the HDPE diffractogram is approximately 83%, a value close to calculated before of about 75% [40]. Although the degree of crystallinity of HDPE is consistent with the previously reported value, it is important to mention that variation may occur, which is attributed to the different processing characteristics of the various types of HDPE [40].

The XRD analysis provided results related to the crystalline phases of the sample. The diffractogram of aluminum can be seen in Figure 5(d). The diffractogram showed the crystallographic planes of aluminum with a cubic structure, identified by the crystallographic file 01-089-4037. The indexed peaks were the same as those found in the work of Li et al. [41]. Upon analysis of Figure 5(d) and comparison of the values, it is evident that the relative intensities differ from those indicated in the file. This disparity is likely due to the nature of the tested sample, which is not a powder, and possibly due to some type of forming process.

3.3. Fourier Transform Infrared Spectroscopy (FTIR)

In this section, the results obtained from the FTIR test of aluminum, HDPE, and the flax and aramid fabrics will be presented.

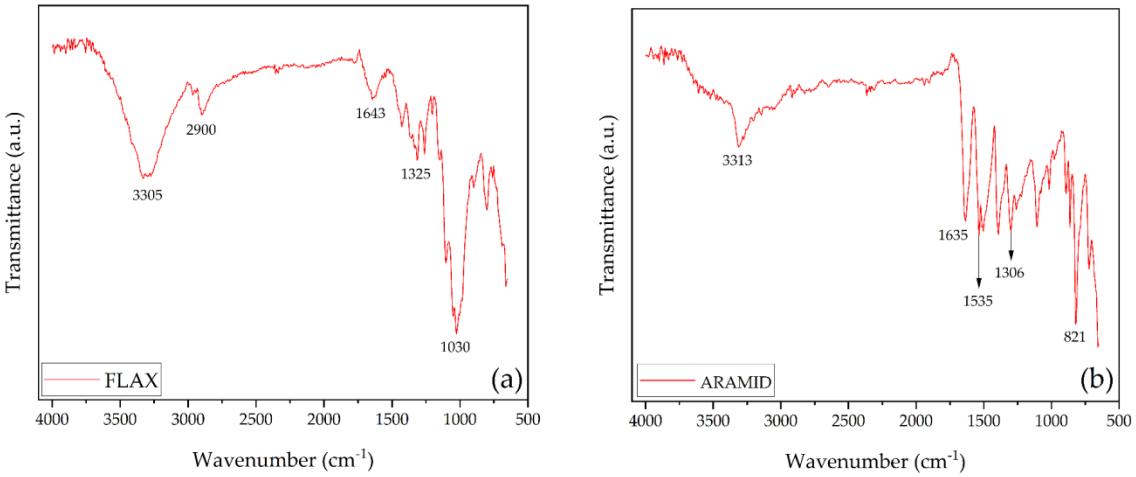

Figure 6. Vibrational spectrum obtained for (a) flax fabric; (b) aramid fabric.

NLFs are mainly composed of cellulose, lignin, and hemicellulose. From the FTIR spectrum it is possible to establish a relationship between the observed bands and the chemical bonds of the fiber, Figure 6(a). The wavenumber associated with the band at 3320 cm^{-1} is assigned to the OH stretching vibration, indicating the presence of hydroxyl groups. The band at 2900 cm^{-1} corresponds to C-H stretching vibrations, typical of both aliphatic and aromatic compounds. The band observed at 1643 cm^{-1} is mainly attributed to the C=O stretching vibration, characteristic of aliphatic carboxylic acids and the ketone group within the cellulose chain. The 1325 cm^{-1} band can be assigned to in-plane OH bending vibrations. Finally, the band at 1030 cm^{-1} is associated with CH and CO deformations [42–47].

In Figure 6(b), a wide band at 3313 cm^{-1} corresponds to the NH stretching, which occurs when carbonyl and amine are in the trans

configuration (Amide-A). The band observed at 1635 cm^{-1} corresponds to the amide I band, related to the C=O stretching vibration. At 1535 cm^{-1}, the amide II band can be observed, which is associated with the coupling between the CN stretching vibration and the NH bending vibration. The band observed at 1306 cm^{-1} is related to the amide III band, which is directly associated with the coupling between the vibrations of the C-N, NH, and C-C bonds. The band observed at cm^{-1} is attributed to vibrations of the aromatic ring [48–52].

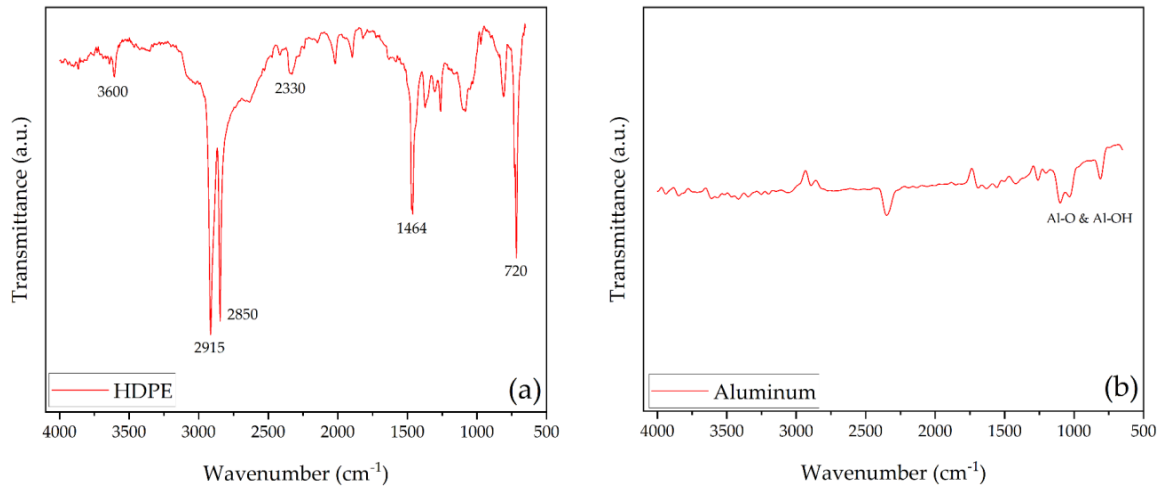

Figure 7. Vibrational spectrum obtained for (a) HDPE; (b) Aluminum

In Figure 7(a), the band found at 2915 cm^{-1} refers to C-H stretching, and the band at wavenumber 2850 cm^{-1} originates from the $=CH_2$ bond and is related to the symmetric stretching of CH (methylene). The band observed at 2330 cm^{-1} originates from C=O stretching attributed to carboxylic stretching. The 1464 cm^{-1} band originates from CH_2 bending caused by the aromatic aryl ring. The sharp band at 720 cm^{-1} is associated with the out-of-plane bending vibration of CH [53–57].

In Figure 7(b), the bands observed up to ≤1200 cm^{-1} result from the bending vibrations of single Al-O and Al-OH bonds. These vibrations are caused by the presence of an oxidized and hydroxylated layer on the surface of the sample [58–60].

3.4. Thermogravimetric Analysis (TGA)

The thermal stability of polymeric materials is essential for defining their operating temperature limit and environmental use conditions, as it is associated with their thermal decomposition temperature and decomposition rate [61]. Through TGA, it was possible to observe the mass loss process of high-density polyethylene, aramid, flax, and aluminum. Figure 8 illustrates the curves resulting from the thermogravimetric test performed on flax and aramid.

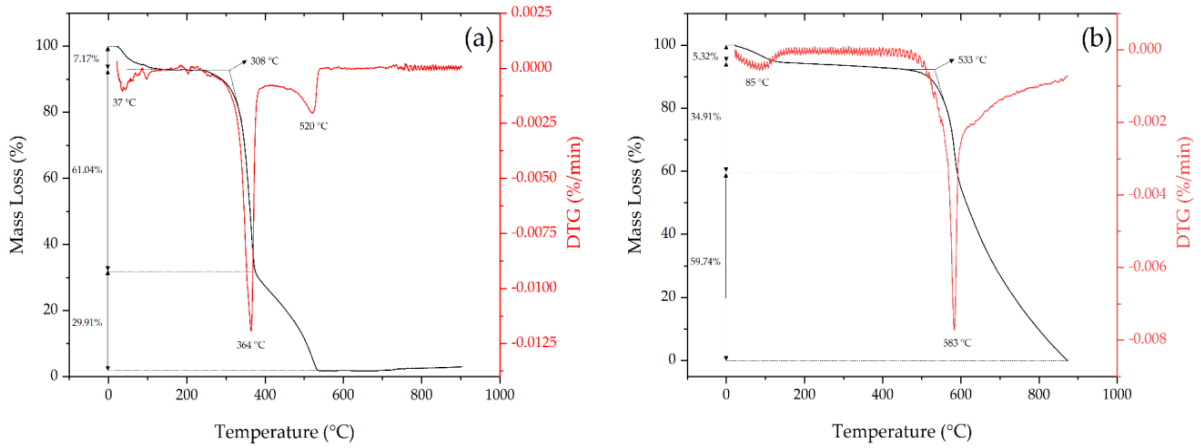

Figure 8. TGA and DTG curves obtained for (a) flax fabric; (b) aramid fabric

The curve presented in Figure 8(a), shows an initial mass loss up to around 150 °C, corresponding to the moisture loss of the material. It is noted that flax undergoes significant degradation in Stage II, which began at 308 °C, as indicated in the graph. The temperature range from 200 to 500 °C coincides with the decomposition temperature of hemicellulose, cellulose, and lignin, which are the main constituents of flax [62]. At 900 °C, an ash content of 1.88% of the total mass was observed.

An initial stage of mass loss of 5.32% is observed up to 200 °C, associated with the loss of moisture of the material, as shown in Figure 8(b). It can be seen that this loss is greater for aramid than for HDPE. This occurs because aramid, although a synthetic material such as HDPE, is more hydrophilic than high-density polyethylene, containing a higher concentration of moisture on its surface. In the work of Meliande et al. [19], this loss is reported to be 6% until the onset of a sharp mass decline at 477 °C. The major thermal decomposition (stages II and III) begins at 533 °C, with a total mass loss of 94.62%, due to degradation of the amide units (II) and primarily due to the decomposition of heterocyclic and aromatic units (III) [63]. Aramid left a residue of 0.06% at 900 °C.

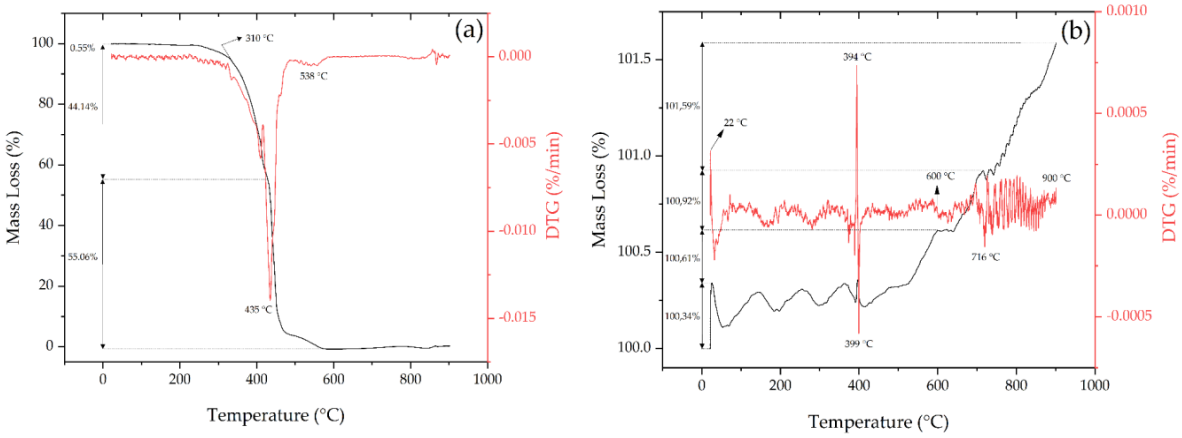

Figure 9. TGA and DTG curves obtained for (a) HDPE; (b) aluminum.

In Figure 9a, an initial mass loss of 0.55% (almost negligible) can be observed. This occurs because of the evaporation of water molecules that are weakly bound to the polymer surface and the dehydration caused by secondary alcohol groups. Volatile emission begins at 310 °C, where the main mass loss related to stages II and III begins, with peaks at 435 °C and 538 °C [64,65].

It is commonly expected that, in an inert atmosphere such as nitrogen, the mass of a sample in a TGA test will remain constant or decrease due to processes such as decomposition or evaporation. However, aluminum (Figure 9b) exhibited a different behavior, with a mass gain during the test (1.59% up to 900 °C). This behavior can be explained by the formation of aluminum nitride (AlN). Although nitrogen is considered inert, it reacts with certain metals at high temperatures, forming solid compounds such as AlN, which adhere to the metal surface.

Another point that may justify this behavior is the presence of an oxidized surface layer, evidenced by XRD and FTIR analysis, which suggests that, in addition to nitridation, oxidation also contributed to the mass gain observed in TGA. Aluminum, when exposed to oxygen at high temperatures, forms aluminum oxide (Al_2O_3), another non-volatile solid compound that contributes to the mass gain of the sample. Therefore, the mass gain observed in the TGA test of aluminum can be attributed to the combination of two processes: the formation of aluminum nitride and the oxidation of the metal, both occurring simultaneously and contributing to the increase in the mass of the sample [66–71].

3.5. Differential Scanning Calorimetry (DSC)

The first endothermic peak for the flax fabrics (Figure 10a) was observed around 58 °C. According to previous works, it corresponds to the loss or evaporation of absorbed water [72]. The temperatures at 372 and 395 °C are endothermic and exothermic peaks, respectively. The first may be attributed to depolymerization of cellulose with the formation of volatiles. The observed exothermic peak is probably due to the degradation of the hemicelluloses present in the samples, as well as the break of the aromatic rings present in the fiber lignin content, which occurs over a wide range of temperatures [72].

For the aramid adopted in this work (Figure 10b), an endothermic peak was observed at around 106 °C, and two additional peaks: an exothermic peak at around 573 °C, and an endothermic one at around 586 °C. The first peak may also be related to the evaporation of absorbed water. Similar results can be observed in a study in which the DSC test was applied to aramid fibers [73].

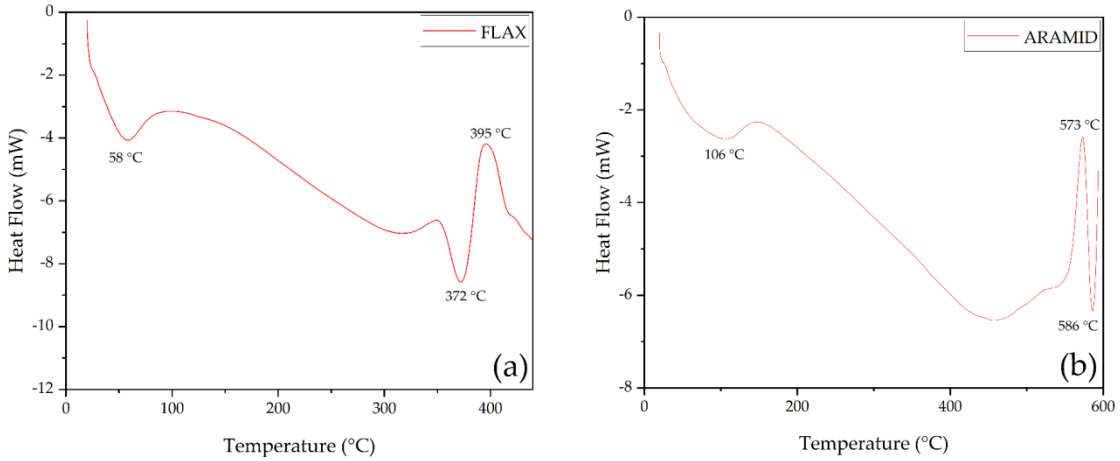

Figure 10. DSC curves for (a) pure flax fabric; (b) as-received aramid fabric sample

The DSC curves for both HDPE in Figure 11(a) and aluminum plates in Figure 11(b) presented only one endothermic peak each. The first is observed around 131 °C, and the second at 562 °C. An exothermic peak for the aluminum plate is observed at around °C. This behavior for HDPE is expected also due to the melting point of the polymeric material, also observed before [74], which would not be possible in a metallic material as the aluminum plates adopted in this work.

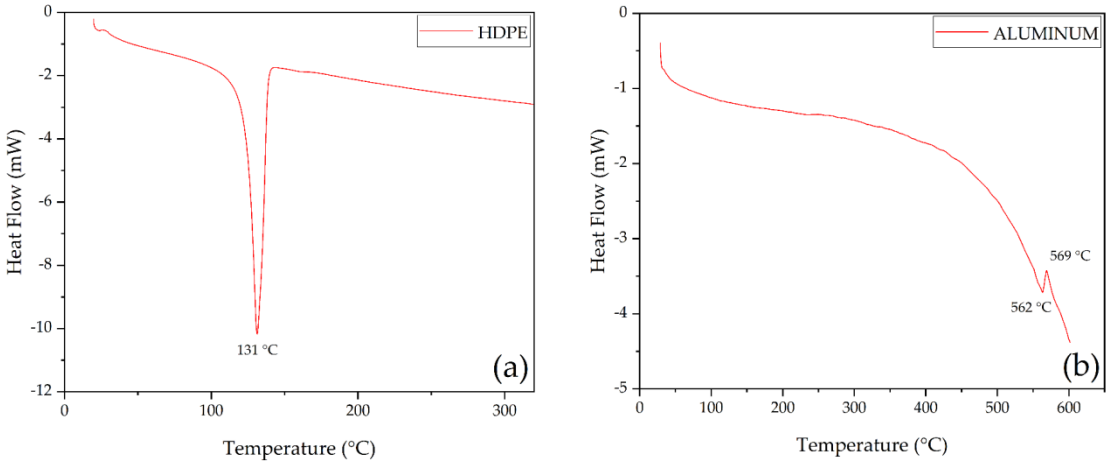

Figure 11. DSC curves for (a) HDPE; (b) aluminum plate sample.

3.6. Final Remarks

The results presented in the present study indicate that the materials investigated show great potential for application in ballistic helmets. The chemical and thermal characterization confirms the viability of these materials at operating temperatures suitable for the conditions required in high-risk military environments.

4. CONCLUSIONS

- FTIR analysis revealed the functional groups present in the studied materials, and these results were corroborated with findings from the literature.
- In the XRD analysis, it was possible to obtain the crystallinity of the materials in this study. The high-density polyethylene (HDPE) and aramid showed results superior to those found in the literature. For flax and aluminum, the results presented are comparable to those reported in the literature.
- The higher crystallinity of the materials obtained in the present work indicates that, when applied to the composite, they may

significantly enhance the mechanical properties of ballistic helmets.

- From the thermogravimetric analysis, it was possible to observe the mass loss of the main constituents of the materials studied.
- The maximum operating temperature of the individually studied materials was determined.
- When used together for the possible manufacture of hybrid composites for ballistic helmets, a working temperature of 200 °C will be adopted, considering that decomposition of the main constituents of flax begins at that point.

Acknowledgements

We thank CAPES and FAPERJ for the essential financial support provided for the development of this research. We also extend our gratitude to IPQM and the Metallurgical and Materials Engineering Program (PEMM) at UFRJ for their technical support, infrastructure, and scientific guidance.

5. REFERENCES

[1] A.L.Marinelli, M.R. Monteiro, J.D.Ambrósio, M.C.Branciforti, M.Kobayashi, A.D. Nobre (2008) Desenvolvimento de compósitos poliméricos com fibras vegetais naturais da biodiversidade: uma contribuição para a sustentabilidade amazônica, Polímeros, 18, 92–99. https://doi.org/10.1590/S0104-14282008000200005

[2] S.N.Monteiro, F. Lopes, A.P. Barbosa, A.Bevitori, I.L. Da Silva, L.L. Da Costa (2011) Natural lignocellulosic fibers as engineering materials—an overview, Metallurgical and Materials Transactions A, 42, 2963–2974. https://doi.org/10.1007/s11661-011-0789-6

[3] E.C.Lustosa, C.H. Menezzi, S.M. Luz, J. Raabe, L.C. Jesus, R.M. Leão, A. Zattera (2020) Propriedades térmicas de compósitos de acrilonitrila-butadieno-estireno (ABS) e fibras de celulose modificadas com nanopartículas de sílica (SiO_2), Matéria (Rio de Janeiro), 25, e–12784. https://doi.org/10.1590/s1517-707620200003.1084

[4] L. Siouta, M. Apostolopoulou, A. Bakolas (2024) Natural Fibers in Composite Materials for Sustainable Building: A State-of-the-Art Review on Treated Hemp Fibers and Hurds in Mortars, Sustainability, 16, 10368. https://doi.org/10.3390/su162310368

[5] B.Z. Dias, C.E.d. Alvarez, L.C. Meneghetti, A.H. Lara (2024) Plant-derived thermosetting composites: water absorption and mechanical properties retention after weathering, AmbienteConstruído, 24, e127325. https://doi.org/10.1590/s1678-86212024000100708

[6] P.H.P.M. da Silveira, B.F.d.A.F. Cardoso, B.Z. Marchi, S.N. Monteiro (2024) Amazon Natural Fibers for Application in Engineering Composites and Sustainable Actions: A Review, Eng, 5, 133–179.https://doi.org/10.3390/eng5010009

[7] T. Islam, M.H. Chaion, M.A. Jalil, A.S. Rafi, F. Mushtari, A.K. Dhar, S. Hossain (2024) Advancements and challenges in natural fiber-reinforced hybrid composites: a comprehensive review, SPE Polymers, 5, 481–506. https://doi.org/10.1002/pls2.10145

[8] N. Nurazzi, M. Asyraf, M. Rayung, M. Norrrahim, S. Shazleen, M. Rani, A. Shafi, H. Aisyah, M. Radzi, F. Sabaruddin, et al. (2021) Thermogravimetric analysis properties of cellulosic natural fiber polymer composites: A review on influence of chemical treatments, Polymers, 13, 2710. https://doi.org/10.3390/polym13162710

[9] H. Aisyah, M. Paridah, S. Sapuan, R. Ilyas, A. Khalina, N. Nurazzi, S. Lee, C. Lee (2021) A comprehensive review on advanced sustainable woven natural fibre polymer composites, Polymers, 13, 471. https://doi.org/10.3390/polym13030471

[10] M. Mohammed, J.K. Oleiwi, A.M. Mohammed, A.J.M. Jawad, A.F. Osman, T. Adam, B.O. Betar, S.C. Gopinath (2024) A Review on the Advancement of Renewable Natural Fiber Hybrid Composites: Prospects, Challenges, and Industrial Applications, Journal of Renewable Materials, 12. https://doi.org/10.32604/jrm.2024.051201

[11] S. Islam, M.B. Hasan, F.E. Karim, M. Kodrić, M.R. Islam, M.M. Khatun, K.A. Motaleb (2025) Thermoset and thermoplastic polymer composites reinforced with flax fiber: Properties and application—A review, SPE Polymers, 6, e10172. https://doi.org/10.1002/pls2.10172

[12] B.Z. Marchi, P.H.P.M. da Silveira, W.B. Almeida Bezerra, M.H.P. da Silva, S.N. Monteiro, A.B.H. da Silva Figueiredo (2024) Evaluation of the thermomechanical properties of novel epoxy composites reinforced with Geonomabaculifera fibers, Scientific Reports, 14, 26565. https://doi.org/10.1038/s41598-024-78449-5

[13] L. de Mendonça Neuba, R. Felipe Pereira Junio, D.S. Silva, A.A. Palmeira, S. Tavares, B. Lazarus, A.C. Pereira, S.N. Monteiro (2024) Thermal, Morphological, and Structural Characterization of Seven-Islands-Sedge (Cyperusmalaccensis) Fiber with Graphene Oxide as a Coupling Agent for Future Polymer Composite Reinforcement, Journal of Natural Fibers, 21, 2392284. https://doi.org/10.1080/15440478.2024.2392284

[14] M.P. Ribeiro, L. de Mendonça Neuba, P.H.P.M. da Silveira, F.S. da Luz, A.B.H. da Silva Figueiredo, S.N. Monteiro, M.O. Moreira (2021) Mechanical, thermal and ballistic performance of epoxy composites reinforced with Cannabis sativa hemp fabric, Journal of Materials Research and Technology, 12, 221–233. https://doi.org/10.1016/j.jmrt.2021.02.064

[15] A. Azevedo, T. Lima, N. Simonassi, M.P. Ribeiro, F. Garcia Filho, S. Monteiro (2022) Piassava fiber: A novel reinforcement for cement-based matrix composites, Concilium, 22, 379–390. https://doi.org/10.53660/clm-150-166

[16] T.T. da Silva, P.H.P.M. da Silveira, M.P. Ribeiro, M.F. Lemos, A.P. da Silva, S.N. Monteiro, L.F.C. Nascimento (2021) Thermal and chemical characterization of kenaf fiber (Hibiscus cannabinus) reinforced epoxy matrix composites, Polymers, 13, 2016. https://doi.org/10.3390/polym13122016

[17] V. Stefanescu, A. Boboc, A. Cojan, R. Bosoanca, C. Muntenita, M. Bunea (2018) The thermal behavior of Hybrid fabric reinforced composites with stratified filled epoxy matrix, Mat. Plast, 55, 161–166. https://doi.org/10.37358/mp.18.2.4986

[18] V. Chinnasamy, S.P. Subramani, S.K. Palaniappan, B. Mylsamy, K. Aruchamy (2020) Characterization on thermal properties of glass fiber and kevlar fiber with modified epoxy hybrid composites, Journal of Materials Research and Technology, 9, 3158–3167. https://doi.org/10.1016/j.jmrt.2020.01.061

[19] N.M. Meliande, M.S. Oliveira, M.F. Lemos, A.C. Pereira, A.B.H. da Silva Figueiredo, S.N. Monteiro, L.F.C. Nascimento (2023) Thermal Behavior of Curaua-Aramid Hybrid Laminated Composites for Ballistic Helmet, Polymers, 15, 3214. https://doi.org/10.3390/polym15153214

[20] L. Tang, M. Jia, M. He, Q. Liu, Y. Lin, Y. Yi, X. Liu, X. Liu, Y. Tang, J. Gu (2024) Fabrication, applications, and prospects for poly(p-phenylenebenzobisoxazole) nanofibers, SusMat, e245. https://doi.org/10.1002/sus2.245

[21] L. Tang, J. Dang, M. He, J. Li, J. Kong, Y. Tang, J. Gu (2019) Preparation and properties of cyanate-based wave-transparent laminated composites reinforced by dopamine/POSS functionalized Kevlar cloth, Composites Science and Technology, 169, 120–126. https://doi.org/10.1016/j.compscitech.2018.11.018

[22] G. Rajesh, H. Kim, T. Setoguchi, S. Raghunathan (2007) Performance analysis and enhancement of the ballistic range, Proceedings of the Institution of Mechanical Engineers, Part G: Journal of Aerospace Engineering, 221, 649–659. https://doi.org/10.1243/09544100jaero229

[23] C. Tham, V. Tan, H.P. Lee (2008) Ballistic impact of a KEVLAR® helmet: Experiment and simulations, International Journal of Impact Engineering, 35, 304–318. https://doi.org/10.1016/j.ijimpeng.2007.03.008

[24] M. Asyraf, M. Suriani, C. Ruzaidi, A. Khalina, R. Ilyas, M. Asyraf, A. Syamsir, A. Azmi, A. Mohamed (2022) Development of natural fibre-reinforced polymer composites ballistic helmet using concurrent engineering approach: a brief review, Sustainability, 14, 7092. https://doi.org/10.3390/su14127092

[25] A. Harmukh, A. Singh, P. Kumar, S.K. Verma, P.D. Kumar, S. Ganpule (2023) Mechanical analysis of helmeted headforms under ballistic impact with implications in performance evaluation of ballistic helmets, Frontiers in Mechanical Engineering, 9, 1270905. https://doi.org/10.3389/fmech.2023.1270905

[26] Y. Li, H. Fan, X.L. Gao (2022) Ballistic helmets: Recent advances in materials, protection mechanisms, performance, and head injury mitigation, Composites Part B: Engineering, 238, 109890. https://doi.org/10.1016/j.compositesb.2022.109890

[27] Y. Liang, X. Chen, C. Soutis (2022) Review on manufacture of military composite helmet, Applied Composite Materials, 29, 305–323. https://doi.org/10.1007/s10443-021-09944-5

[28] Y. Li, K. Adanty, P. Vakiel, S. Ouellet, A.H. Vette, D. Raboud, C.R. Dennison (2023) Review of mechanisms and research methods for blunt ballistic head injury, Journal of Biomechanical Engineering, 145, 010801. https://doi.org/10.1115/1.4055289

[29] ASTM D3776 (2020) Standard test methods for mass per unit area (weight) of fabric, ASTM D3776-20.

[30] H. Klug (1974) X-ray diffraction procedures for polycrystalline and amorphous materials.

[31] R. Jenkins, T. Fawcett, D. Smith, J. Visser, M. Morris, L. Frevel (1986) JCPDS—International Centre for Diffraction Data Sample Preparation Methods in X-Ray Powder Diffraction, Powder Diffraction, 1, 51–63. https://doi.org/10.1017/s0885715600011581

[32] L. Segal, J. Creely, A. Martin Jr, C. Conrad (1959) An empirical method for estimating the degree of crystallinity of native cellulose using the X-ray diffractometer, Textile Research Journal, 29, 786–794. https://doi.org/10.1177/004051755902901003

[33] A.R. Martin, M.A. Martins, L.H. Mattoso, O.R. Silva (2009) Caracterização química e estrutural de fibra de sisal da variedade Agave sisalana, Polímeros: Ciência e Tecnologia, 19, 40–46. https://doi.org/10.1590/s0104-14282009000100011

[34] M.P. Ribeiro, P.H.P.M. da Silveira, F. de Oliveira Braga, S.N. Monteiro (2022) Fabric impregnation with shear thickening fluid for ballistic armor polymer composites: an updated overview, Polymers, 14, 4357. https://doi.org/10.3390/polym14204357

[35] V. Mahesh, D. Harursampath, V. Mahesh (2022) An experimental study on ballistic impact response of jute reinforced polyethylene glycol and nano silica based shear thickening fluid composite, Defence Technology, 18, 401–409. https://doi.org/10.1016/j.dt.2021.03.013

[36] C. Teng, H. Li, J. Liu, H. Gu, H. Kong, M. Yu (2020) Effect of high molecular weight PPTA on liquid crystalline phase and spinning process of aramid fibers, Polymers, 12, 1206. https://doi.org/10.3390/polym12051206

[37] M. Ramesh (2019) Flax (Linumusitatissimum L.) fibre reinforced polymer composite materials: A review on preparation, properties and prospects, Progress in Materials Science, 102, 109–166. https://doi.org/10.1016/j.pmatsci.2018.12.004

[38] Z. Sui, Z. Guo, Y. Li, Q. Zhang, B. Zu, X. Zhao (2023) Study on preparation and performance of multifunctional linen fabric finishing agent, Textile Research Journal, 93, 1686–1698. https://doi.org/10.1177/00405175221134974

[39] G.M. Gonzalez, J. Ward, J. Song, K. Swana, S.A. Fossey, J.L. Palmer, F.W. Zhang, V.M. Lucian, L. Cera, J.F. Zimmerman, et al. (2020) Para-aramid fiber sheets for simultaneous mechanical and thermal protection in extreme environments, Matter, 3, 742–758. https://doi.org/10.1016/j.matt.2020.06.001

[40] G. de Almeida Santos da Silva, J.R.M. d'Almeida, S. Letichevsky, R.R. de Avillez (2023) Crystallinity and rheology of HDPE/PA12 blends compatibilized with HDPE-alt-MAH, Polymers for Advanced Technologies. https://doi.org/10.1002/pat.5873

[41] J. Li, G. Wang, M. Zhang, J. Li, X. Fang, X. Ma (2023) Strengthening mechanisms of a heterostructured pure aluminum with extraordinary mechanical properties, Materials Characterization, p. 113049. https://doi.org/10.1016/j.matchar.2023.113049

[42] D. Ray, B. Sarkar (2001) Characterization of alkali-treated jute fibers for physical and mechanical properties, Journal of Applied Polymer Science, 80, 1013–1020. https://doi.org/10.1002/app.1184

[43] P. Jandas, S. Mohanty, S. Nayak (2012) Renewable resource-based biocomposites of various surface treated banana fiber and poly lactic acid: characterization and biodegradability, Journal of Polymers and the Environment, 20, 583–595. https://doi.org/10.1007/s10924-012-0415-8

[44] S. Huo, C.A. Ulven, H. Wang, X. Wang (2013) Chemical and mechanical properties studies of Chinese linen flax and its composites, Polymers and Polymer Composites, 21, 275–286. https://doi.org/10.1177/096739111302100502

[45] X. Xia, W. Liu, L. Zhou, Z. Hua, H. Liu, S. He (2016) Modification of flax fiber surface and its compatibilization in polylactic acid/flax composites, Iranian Polymer Journal, 25, 25–35. https://doi.org/10.1007/s13726-015-0395-3

[46] R.H.M. Reis, V.S. Cândido, L.F. Nunes, S.N. Monteiro (2019) Chemical and Morphological Characterization of Guaruman Fiber, In Green Materials Engineering; Springer, pp. 107–113. https://doi.org/10.1007/978-3-030-10383-5_12

[47] N.Q. Khuyen, P.V.D. Han, N.T. Nguyen, Q.B. Le, M. Harjo, G. Anbarjafari, R. Kiefer, T. Tamm (2021) The Use of Laminates of Commercially Available Fabrics for Anti-Stab Body-Armor, Polymers, 13, 1077. https://doi.org/10.3390/polym13071077

[48] J. Zhao (2013) Effect of surface treatment on the structure and properties of para-aramid fibers by phosphoric acid, Fibers and Polymers, 14, 59–64. https://doi.org/10.1007/s12221-013-0059-x

[49] Z. Li, X. Cheng, S. He, X. Shi, L. Gong, H. Zhang (2016) Aramid fibers reinforced silica aerogel composites with low thermal conductivity and improved mechanical performance, Composites Part A: Applied Science and Manufacturing, 84, 316–325. https://doi.org/10.1016/j.compositesa.2016.02.014

[50] S. Anidha, N. Latha, M. Muthukkumar (2019) Reinforcement of aramid fiber with bagasse epoxy bio-degradable composite: investigations on mechanical properties and surface morphology, Journal of Materials Research and Technology, 8, 3198–3212. https://doi.org/10.1016/j.jmrt.2019.05.008

[51] R.F. Nascimento, A.O. da Silva, R.P. Weber, S.N. Monteiro (2020) Influence of UV radiation and moisture associated with natural weathering on the ballistic performance of aramid fabric armor, Journal of Materials Research and Technology, 9, 10334–10345. https://doi.org/10.1016/j.jmrt.2020.07.046

[52] E.A. Siddig, X. Yu, H. Tao, G. Ming, Y. Baojing, W. Tianshu, J. Zhang (2020) Plasma-induced graft polymerization on the surface of aramid fabrics with improved omniphobicity and washing durability, Plasma Science and Technology, 22, 055503. https://doi.org/10.1088/2058-6272/ab65dd

[53] N.M. Stark, L.M. Matuana (2004) Surface chemistry changes of weathered HDPE/wood-flour composites studied by XPS and FTIR spectroscopy, Polymer Degradation and Stability, 86, 1–9. https://doi.org/10.1016/j.polymdegradstab.2003.11.002

[54] V. Parthasarathi, B. Sundaresan, V. Dhanalakshmi, R. Anbarasan (2010) Functionalization of HDPE with aminoester and hydroxyester by thermolysis method—An FTIR-RI approach, Thermochimica Acta, 510, 61–67. https://doi.org/10.1016/j.joei.2019.09.003

[55] R.K. Singh, B. Ruj, A.K. Sadhukhan, P. Gupta (2020) A TG-FTIR investigation on the co-pyrolysis of the waste HDPE, PP, PS and PET under high heating conditions, Journal of the Energy Institute, 93, 1020–1035.

[56] M. Saleh, Z. Al-Hajri, A. Popelka, S. Javaid Zaidi (2020) Preparation and characterization of alumina HDPE composites, Materials, 13, 250. https://doi.org/10.3390/ma13010250

[57] J. Li, X. Yao, S. Chen, K. Xu, B. Fan, D. Yang, L. Geng, H. Qiao (2022) Investigation on the co-pyrolysis of agricultural waste and high-density polyethylene using TG-FTIR and artificial neural network modelling, Process Safety and Environmental Protection, 160, 341–353. https://doi.org/10.1016/j.psep.2022.02.033

[58] S. Sivakumar, J. Sivasubramanian, B. Raja (2012) Aluminium-induced structural, metabolic alterations and protective effects of desferrioxamine in the brain tissue of mice: an FTIR study, Spectrochimica Acta Part A: Molecular and Biomolecular Spectroscopy, 99, 252–258.

[59] https://doi.org/10.1016/j.saa.2012.09.036

[60] D.K. Kozlica, A. Kokalj, I. Milošev (2021) Synergistic effect of 2-mercaptobenzimidazole and octylphosphonic acid as corrosion inhibitors for copper and aluminium – An electrochemical, XPS, FTIR and DFT study, Corrosion Science, 182, 109082. https://doi.org/10.1016/j.corsci.2020.109082

[61] M.H. Adib, R. Abedinzadeh (2023) Study of mechanical properties and wear behavior of hybrid Al/(Al_2O_3 + SiC) nanocomposites fabricated by powder technology, Materials Chemistry and Physics, 305, 127922. https://doi.org/10.1016/j.matchemphys.2023.127922

[62] S. Kumar, R. Singh (2014) Pyrolysis kinetics of waste high-density polyethylene using thermogravimetric analysis, International Journal of ChemTech Research, 6, 131–137.

[63] R. Agarwal, P. Das, S.R. Chowdhury (2024) Gamma radiation-assisted functionalization of flax fibers for diversified applications, Journal of Radioanalytical and Nuclear Chemistry, pp. 1–8. https://doi.org/10.1007/s10967-023-09310-8

[64] C. Chen, X. Wang, F. Wang, T. Peng (2020) Preparation and characterization of para-aramid fibers with the main chain containing heterocyclic units, Journal of Macromolecular Science, Part B, 59, 90–99. https://doi.org/10.1080/00222348.2019.1694754

[65] S.A. Al-Bayaty, R.A. Al-Uqaily, S. Hameed (2020) Study of thermal degradation kinetics of high-density polyethylene (HDPE) by using TGA

technique, In Proceedings of the AIP Conference 1Proceedings. AIP Publishing, Vol. 2290. https://doi.org/10.1063/5.0027503
[66] S. Bahlouli, A. Belaadi, A. Makhlouf, H. Alshahrani, M.K. Khan, M. Jawaid (2023) Effect of fiber loading on thermal properties of cellulosic Washingtonia reinforced HDPEbiocomposites, Polymers, 15, 2910. https://doi.org/10.3390/polym15132910
[67] K. Vlach, O. Salas, H. Ni, V. Jayaram, C. Levi, R. Mehrabian (1991) A thermogravimetric study of the oxidative growth of Al_2O_3/Al alloy composites, Journal of Materials Research, 6, 1982–1995. https://doi.org/10.1557/jmr.1991.1982
[68] R. Bernst, A. Schneider, M. Spiegel (2006) Metal dusting of binary iron aluminium alloys at 600 °C, Materials and Corrosion, 57, 724–728. https://doi.org/10.1002/maco.200503955
[69] D. Stevens, A. Kvithyld, T.A. Engh (2011) Oxidation of rolled and flash anodized 3000 aluminum in air, nitrogen, oxygen, and carbon dioxide atmospheres, In Proceedings of the Materials Science Forum. Trans Tech Publ, Vol. 693, pp. 63–70. https://doi.org/10.4028/www.scientific.net/msf.693.63
[70] S.I. Castañeda, F.J. Pérez (2018) High performance of Al–Si–CVD–FBR coating on P92 steel against steam oxidation at 650 °C: Part 1, Materials and Corrosion, 69, 307–318. https://doi.org/10.1002/maco.201709600
[71] C.K.W. Solem, E. Solberg, G. Tranell, R.E. Aune (2021) Influence of Mg concentration on the inhibiting effect of CO_2 on the rate of oxidation of aluminum alloys 5182 and 6016, In Proceedings of the Light Metals: 50th Anniversary Edition. Springer, pp. 742–750. https://doi.org/10.1007/978-3-030-65396-5_97
[72] Q. Huang, S. Yu, Y. Chen, S. Lu, Z. Lu, C. Liu (2022) Study on the high temperature oxidation/nitridation behavior of Mg alloys AZ31, WE43 and ZE10, Case Studies in Thermal Engineering, 30, 101759. https://doi.org/10.1016/j.csite.2022.101759
[73] M.M. Kabir, M.Y. Alhaik, S.H. Aldajah, K.T. Lau, H. Wang, M.M. Islam (2021) Effect of hemp fibre surface treatment on the fibre–matrix interface and the influence of cellulose, hemicellulose, and lignin contents on composite strength properties, Advances in Materials Science and Engineering, 9753779. https://doi.org/10.1155/2021/9753779
[74] Q. Guoquan, W. Yin, Q. Dongtao, W. Bin, L. Houbu, D. Nan, C. Xuehua (2016) Experimental study on the thermostable property of aramid fiber reinforced PE-RT pipes, Natural Gas Industry B. https://doi.org/10.1016/j.ngib.2015.09.023
[75] D. Li, L. Zhou, X. Wang, L. He, X. Yang (2019) Effect of crystallinity of polyethylene with different densities on breakdown strength and conductance property, Materials, 12, 1746. https://doi.org/10.3390/ma12111746

IZVOD

HEMIJSKA I TERMIČKA ANALIZA LANA, ARAMIDA I ALUMINIJUMA ZA HDPE KOMPOZITE U ZAŠTITNIM ŠLEMOVIMA

Uočava se sve veće interesovanje za upotrebu održivih materijala kao ojačanja u polimernim kompozitima, uključujući i balističke šlemove koje koriste vojne snage. Tipični primeri su prirodna lignocelulozna vlakna (NLF), koja se primenjuju kao ojačanje laganih, ekonomičnih i ekološki prihvatljivih kompozita u poređenju sa sintetičkim vlaknima kao što su staklo, ugljenik i aramid. Njihova fizička i mehanička svojstva variraju u zavisnosti od porekla i karakteristika vlakana, što utiče na njihovu primenu. Hibridizacija poboljšava svojstva kompozita, što dovodi do istraživanja različitih materijala za ojačanje. Ova studija karakteriše aluminijum, kao i tkanine od lana, NLF i aramida, kombinovane sa polietilenom visoke gustine (HDPE), kao matricu kompozita koristeći infracrvenu spektroskopiju sa Furijeovom transformacijom (FTIR), difrakciju X-zraka (XRD), termogravimetrijsku analizu (TGA) i diferencijalnu skenirajuću kalorimetriju (DSC) za moguću primenu kao hibridni kompoziti. U FTIR analizi, materijali su pokazali funkcionalne grupe kompatibilne sa onima opisanim u literaturi. Pored toga, aramid i HDPE su pokazali veće vrednosti kristalnosti od približno 69% i 83%, respektivno. Na osnovu rezultata TGA i DSC analize, bilo je moguće odrediti pojedinačnu radnu temperaturu materijala, koja je bila oko 200 °C, i uzeti je u obzir za moguće kompozite. Ovi nalazi su kompatibilni sa zahtevima za balističke kacige povezanim sa radiološkom zaštitom.

Ključne reči: *Karakterizacija; Furijeova transformaciona infracrvena spektroskopija; rendgenski difraktogram; termogravimetrijska analiza; diferencijalna skenirajuća kalorimetrija*

Naučni rad
Rad primljen: 02.06.2025.
Rad prihvaćen:12.06.2025.

- **Thuane T. da Silva:** 0000-0002-0644-3633
- **Matheus P. Ribeiro:** 0000-0002-4198-7919
- **Lucas de M. Neuba:** 0000-0002-0935-4468
- **Ana P. da Silva:** 0009-0007-2377-6580
- **Sergio N. Monteiro:** 0000-0003-1208-1234

- **Marcos P. C. de Medeiros:** 0000-0001-8504-4341
- **Lucio F. C. Nascimento:** 0000-0003-3484-145X